

## Modeling Combined Diffraction-Refraction in a Coastal Spectral Wave Model

Lihwa Lin and Zeki Demirbilek  
 US Army Engineer Research and Development Center  
 Vicksburg, Mississippi, USA

### ABSTRACT

This paper describes the derivation and implementation of combined wave diffraction-refraction in a spectral directional wave model for coastal applications. The wave refraction is included in the total derivative of wave-action while diffraction is formulated as wave energy diffusion in the wave-action balance equation. The combined diffraction-refraction model equation conserves the total wave-action under no net energy gain or loss. The numerical solution scheme for the model equation is simple and computation is stable. The method is demonstrated in a two-dimensional (2D) steady-state spectral model for a long wedge, an idealized shoal and a coastal harbor physical model.

KEY WORDS: Wave; spectrum; diffraction; refraction; modeling.

### INTRODUCTION

Wave diffraction theory for the interaction with structures has been studied by many researchers in the past following the early work by Sommerfeld (1896). Combined wave diffraction-refraction is more challenging mathematically and analytical solutions are scarce (Penny and Price, 1944). The original work for combined diffraction-refraction by Berkhoff (1972, 1982) and recent investigations are mainly based on either Boussinesq or Mild-slope equation (Nwogu and Demirbilek, 2001) using phase-resolving wave models that require advanced numerical techniques to calculate solutions. Because the phase-resolving models are computationally intensive, their applications are often limited to local small areas. For larger coastal areas, the spectral wave models that neglect wave phase calculations are popular as they are computationally more efficient than the phase-resolving models. However, the implementation of wave diffraction in today's coastal spectral wave models is more or less based on empirical treatment or simple formulation extending the features of phase-resolving models (Chawla et al. 1998; Mase, 2001). The present paper describes a theoretical derivation of wave diffraction combined with wave refraction for spectral wave models. The approach of diffraction formulation is consistent with the well-known Helmholtz equation, and its implementation in the wave action balance equation conserves wave energy for combined diffraction-refraction.

### THEORETICAL BACKGROUND

#### Diffraction Equation

Under the linear wave theory and irrotational motion assumptions for an incompressible fluid, the general solution form of three-dimensional velocity potential  $\phi$  with a uniform depth  $h$  and constant frequency  $\sigma$  in a Cartesian coordinate system  $(x, y, z)$  is

$$\phi(x, y, z) = Z(z)F(x, y)e^{i\sigma t} \quad (1)$$

where  $Z(z) = \frac{g \cosh k(h+z)}{\sigma \cosh kh}$  is the vertical dependency,  $k = \text{wave-length}/2\pi$  is wave number,  $F(x, y)$  is the horizontal dependency,  $e^{i\sigma t}$  is the time dependency for periodic motion with frequency  $\sigma$ , and  $i = \sqrt{-1}$ . Substituting Eq. 1 into the Laplace equation  $\nabla^2 \phi = 0$  for the fluid motion under surface water waves yields the Helmholtz equation in  $F = F(x, y)$  as

$$\frac{\partial^2 F}{\partial x^2} + \frac{\partial^2 F}{\partial y^2} + k^2 F = 0 \quad (2)$$

The solution  $F$  is a complex function and can be expressed as  $F = |F| e^{i\alpha}$  where the magnitude  $|F|$  is the wave amplitude and  $\alpha$  is the wave phase in space. The directional wave energy density  $E = E(x, y, \theta)$  is related to  $F$  as  $E = |F|^2$  and  $F^2 = E e^{i2\alpha}$ .

Multiplying  $2F$  to Eq. 2 yields

$$\frac{\partial^2 F^2}{\partial x^2} + \frac{\partial^2 F^2}{\partial y^2} - 2\left(\frac{\partial F}{\partial x}\right)^2 - 2\left(\frac{\partial F}{\partial y}\right)^2 + 2k^2 F^2 = 0 \quad (3)$$

Recall  $\phi$  satisfies the dynamic free surface boundary condition (DFSBC) at the water surface  $\eta(x, y, t)$ :

$$-\frac{\partial \phi}{\partial t} + \frac{1}{2} \left[ \left( \frac{\partial \phi}{\partial x} \right)^2 + \left( \frac{\partial \phi}{\partial y} \right)^2 \right] + g\eta = 0 \quad \text{on } z = \eta \quad (4)$$

Substituting Eq. 1 into Eq. 4 and linearizing the DFSBC lead to

$$\left( \frac{\partial F}{\partial x} \right)^2 + \left( \frac{\partial F}{\partial y} \right)^2 = 0 \quad (5)$$

Combining Eqs. 3 and 5 yields the Helmholtz equation in  $F^2$  as

$$\frac{\partial^2 F^2}{\partial x^2} + \frac{\partial^2 F^2}{\partial y^2} + 2k^2 F^2 = 0 \quad (6)$$

For spectral wave diffraction, Eq. 6 can be divided into real and imaginary parts by using the expression of  $F^2 = E e^{i(kx \cos \theta + ky \sin \theta)}$ , where  $\theta = \theta(x, y)$  is wave propagation direction. The imaginary part represents the convection of wave energy or wave-action transport in the wave energy or wave-action balance equation. The real part is

$$\frac{\partial^2 E}{\partial x^2} + \frac{\partial^2 E}{\partial y^2} + G(x, y, \theta) k^2 E = 0 \quad (7)$$

or

$$\frac{\partial^2 N}{\partial x^2} + \frac{\partial^2 N}{\partial y^2} + G(x, y, \theta) k^2 N = 0 \quad (8)$$

where  $G(x, y, \theta)$  is related to the wave energy spreading from diffraction and  $N = E / \sigma$  is the wave-action.

### Wave-Action Balance Equation

For coastal spectral wave models, the wave-action balance equation is

$$\frac{dN}{dt} = \frac{\partial N}{\partial t} + \frac{\partial c_{gx} N}{\partial x} + \frac{\partial c_{gy} N}{\partial y} + \frac{\partial c_{g\theta} N}{\partial \theta} = S_{nl} + S_{in} + S_{out} \quad (9)$$

where  $c_{gx} = c_g \cos \theta$  and  $c_{gy} = c_g \sin \theta$  are  $x$  and  $y$  components,

respectively, of the wave group  $c_g = \frac{\partial \sigma}{\partial k}$ , and

$$c_{g\theta} = \frac{c_g}{k} \left( \frac{\partial k}{\partial y} \cos \theta - \frac{\partial k}{\partial x} \sin \theta \right)$$

represents the rate of wave-action transport with respect to direction by wave refraction. Eq. 9 states that the total change of wave-action  $dN / dt$  is balanced by the source function  $S_{in}$ , sink function  $S_{out}$ ,

and non-linear  $S_{nl}$  terms. While the source and sink functions can add and dissipate energy, the non-linear function  $S_{nl}$  including wave diffraction and wave-wave interaction will conserve the wave-action. In the case that both sink and source functions are absent, the total wave energy and wave-action are conserved regardless diffraction, refraction, or non-linear wave-wave interaction occurs or not.

## COMBINED REFRACTION-DIFFRACTION

### Formulation

Applying Eqs. 7 or 8 for spectral wave diffraction is not straight forward because the function  $G$  involves diffraction direction that is part of the solution. Because  $E = |F|^2$  and by comparing Eqs. 2 and 7, the value of  $G$  should fall between 1 and 2, depending on monochromatic or narrow-band spectrum and locations. A valid function  $G$  should conserve wave energy in Eq. 7 and this condition can exist only if  $G$  is a result of diffusion of wave energy in direction defined as

$$\varepsilon \frac{\partial^2 E}{\partial \theta^2} = G(x, y, \theta) E \quad (10)$$

where  $\varepsilon$  is the efficiency of diffusion.

A simple example for Eq. 10 is a symmetric directional distribution of wave energy in the form of

$$\hat{E}(x, y, \theta) = E_o(x, y) \hat{H}(\theta) \quad (11)$$

with the directional spreading function  $\hat{H}(\theta)$  described by a  $\text{sech}^2$  distribution (Donelan et al. 1985) as

$$\hat{H}(\theta) = \frac{\beta}{2} \text{sech}^2(\beta\theta) \quad (12)$$

where  $\beta(x, y)$ , a positive number, is a scaling factor. Eqs. 11 and 12 satisfy the following conditions:

$$\int_{-\pi}^{\pi} \hat{H}(\theta) d\theta = 1 \quad \text{and} \quad \int_{-\pi}^{\pi} \hat{E} d\theta = \int_{-\pi}^{\pi} E_o \hat{H}(\theta) d\theta = E_o \quad (13)$$

where  $E_o$  is the total local spectral energy density.

Because

$$\begin{aligned} \frac{\partial^2 \hat{H}(\theta)}{\partial \theta^2} &= \frac{\partial^2}{\partial \theta^2} \left[ \frac{\beta}{2} \text{sech}^2(\beta\theta) \right] = \beta^3 \frac{\text{sech}^4(\beta\theta)}{\text{sech}(2\beta\theta)} \\ &= 2\beta^2 \frac{\text{sech}^2(\beta\theta)}{\text{sech}(2\beta\theta)} \hat{H}(\theta), \end{aligned} \quad (14)$$

and use the identity  $\text{sech}^2(\beta\theta) = \frac{2 \text{sech}(2\beta\theta)}{1 + \text{sech}(2\beta\theta)}$ ,

Eq. 14 can be rewritten as

$$\frac{\partial^2 \hat{H}(\theta)}{\partial \theta^2} = \hat{H}(\theta) \frac{4\beta^2}{1+\text{sech}(2\beta\theta)}.$$

Accordingly, Eq. 10 can be expressed as

$$\begin{aligned} \varepsilon \frac{\partial^2 \hat{E}}{\partial \theta^2} &= \varepsilon E_o \frac{\partial^2 \hat{H}(\theta)}{\partial \theta^2} = E_o \hat{H}(\theta) \frac{4\varepsilon\beta^2}{1+\text{sech}(2\beta\theta)} \\ &= \frac{4\varepsilon\beta^2}{1+\text{sech}(2\beta\theta)} \hat{E} \end{aligned} \quad (15)$$

and the corresponding  $G$  in Eq. 10 is

$$G(x, y, \theta) = \frac{4\varepsilon\beta^2}{1+\text{sech}(2\beta\theta)} \quad (16)$$

Because  $\text{sech}$  has a range between 0 and 1, the valid  $\varepsilon\beta^2$  values should be between 1/4 and 1. Typically,  $\hat{H}(\theta)$  has a narrow distribution with  $\beta = 30$  to 100 and, accordingly,  $\varepsilon \sim 10^{-3}$  to  $10^{-4}$ .

### Governing Equation

For non-flat bottom, it is necessary to include the transport rate of wave-action as

$$\varepsilon \left\{ \frac{\partial}{\partial x} \left( \frac{c_g}{k} \frac{\partial N}{\partial x} \right) + \frac{\partial}{\partial y} \left( \frac{c_g}{k} \frac{\partial N}{\partial y} \right) + c_g k \frac{\partial^2 N}{\partial \theta^2} \right\} = 0 \quad (17)$$

The above equation represents wave diffraction contribution to the non-linear function  $S_{nl}$  in Eq. 9. By excluding non-linear wave-wave interactions, the wave-action balance equation can be rewritten as

$$\begin{aligned} \frac{dN}{dt} &= \frac{\partial N}{\partial t} + \frac{\partial c_{gx} N}{\partial x} + \frac{\partial c_{gy} N}{\partial y} + \frac{\partial c_{g\theta} N}{\partial \theta} \\ &= \frac{\varepsilon}{\sigma} \left\{ \frac{\partial}{\partial x} \left( cc_g \frac{\partial N}{\partial x} \right) + \frac{\partial}{\partial y} \left( cc_g \frac{\partial N}{\partial y} \right) + cc_g \frac{\partial^2 N}{\partial \theta^2} \right\} \\ &+ S_{in} + S_{out} \end{aligned} \quad (18)$$

where  $c = \sigma / k$  is wave celerity and  $\varepsilon$  is in the order of  $10^{-4}$ .

### NUMERICAL SIMULATIONS

Eq. 18 with the combined diffraction-refraction formulation is demonstrated by numerical computations. A 2D steady-state spectral model in the Coastal Modeling System (Lin et al. 2008) is applied for the demonstration. The model employs a forward-marching, finite-difference method to solve the wave-action balance equation (Mase, 2001) in a rectangular grid. It operates on a coastal half-plane of  $x \geq 0$  that primary waves propagate only from the seaward boundary toward shore. The seaward reflection is calculated by a backward marching after the forwarding-marching calculation is completed. The full-plane mode combines solutions from running two half-plane wave

transformations, where each solution covers the wave direction exactly opposite to the other half-plane wave transformation.

The numerical computation is based on an upwind implicit scheme for solving the wave-action discretized in frequency, direction, and space (Mase, 2001). The formulation for diffraction terms associated with  $\frac{\partial}{\partial y} (cc_g \frac{\partial N}{\partial y})$  and  $\partial^2 N / \partial \theta^2$  in the numerical scheme is

straight forward. The formulation for  $\partial N / \partial x$  and  $\partial(c_{gx} N) / \partial x$  in the primary wave propagation direction is based on the backward difference algorithm. The forward difference term  $\partial N / \partial x$  associated with the diffraction is assumed to be small and thus neglected in the calculation.

The model calculates monochromatic and random waves using the following relation between the total spectral energy density  $E_o$  and wave height  $H_s$ :

$$H_s = \sqrt{8(1 + \lambda^2) E_o} \quad (19)$$

where  $\lambda = \sqrt{1 - \frac{m_2^2}{m_o m_4}}$  is the bandwidth parameter of a spectrum

(Cartwright and Longuet-Higgins, 1956) and  $m_\ell = \int \sigma^\ell E(\sigma) d\sigma$  is the  $\ell$  th moment of the spectrum. For  $\ell = 0$ ,  $m_o = E_o$  and  $\lambda$  value is between 0 (monochromatic wave) and 1 (broad-banded spectrum).

Numerical examples are given in the following subsections for a long wedge, an idealized shoal, and a coastal harbor physical model. These model simulations are used for the demonstration purpose because the spectral wave models can only calculate changes in the local wave energy content and transport but not the wave phase information. The model wave height computed by Eq. 19 essentially reveals the local wave energy level and by no means represents the wave height observed in the physical model or measured in the field. The difference between model calculated wave height and data is evident behind a shoal or in front of a reflective wall that full or partial standing waves occur with crossing waves from different directions.

### An Infinite Wedge

Analytical solution for monochromatic unidirectional incident waves interacting with a fully-reflective vertical wedge of any angle on a flat bottom is available (Chen, 1987). The wave model domain was a square grid of 2,010 m  $\times$  2,010 m consisting of 201  $\times$  201 cells with cell size of 10 m  $\times$  10 m and a uniform water depth of 1,000 m. The vertex of the wedge is located at the center cell of the grid. The vertical wedge was represented by dry cells with an elevation of 2 m. The incident wave height is 1 m, and the wave period is 8 sec (0.125 Hz) corresponding to a wavelength of approximately 100 m. The spectral wave transformation is computed on 10-frequency bins (0.06 to 0.15 Hz with 0.01-Hz increment) and 35-direction bins (covering a half-plane with 5-deg spacing). The incident total wave energy density was placed in one directional and frequency bin to represent the monochromatic unidirectional waves for the boundary condition.

Numerical simulations were conducted for a semi-infinite fully reflective breakwater (wedge angle = 0 deg) with incident waves from 90-deg (normal to breakwater) and from 135-deg oblique direction. The model simulated the diffraction with  $\epsilon = 0.0001$ . Figs. 1 and 2 show the comparison of model wave height with the analytical solution (Chen, 1987) for incident waves with 90-deg and 135-deg approach directions, respectively. Because the incident wave height is 1 m, the wave height contours shown in Figs. 1 and 2 are the same as normalized by incident wave height. The model calculates the resultant wave direction by averaging the spectral components from different directions. If fully reflected waves are opposite to incident waves, the model wave direction is reported as the incident wave direction. This occurs in Fig. 1 for incident waves normal to the breakwater as reflected waves combine incident waves in front of the breakwater.

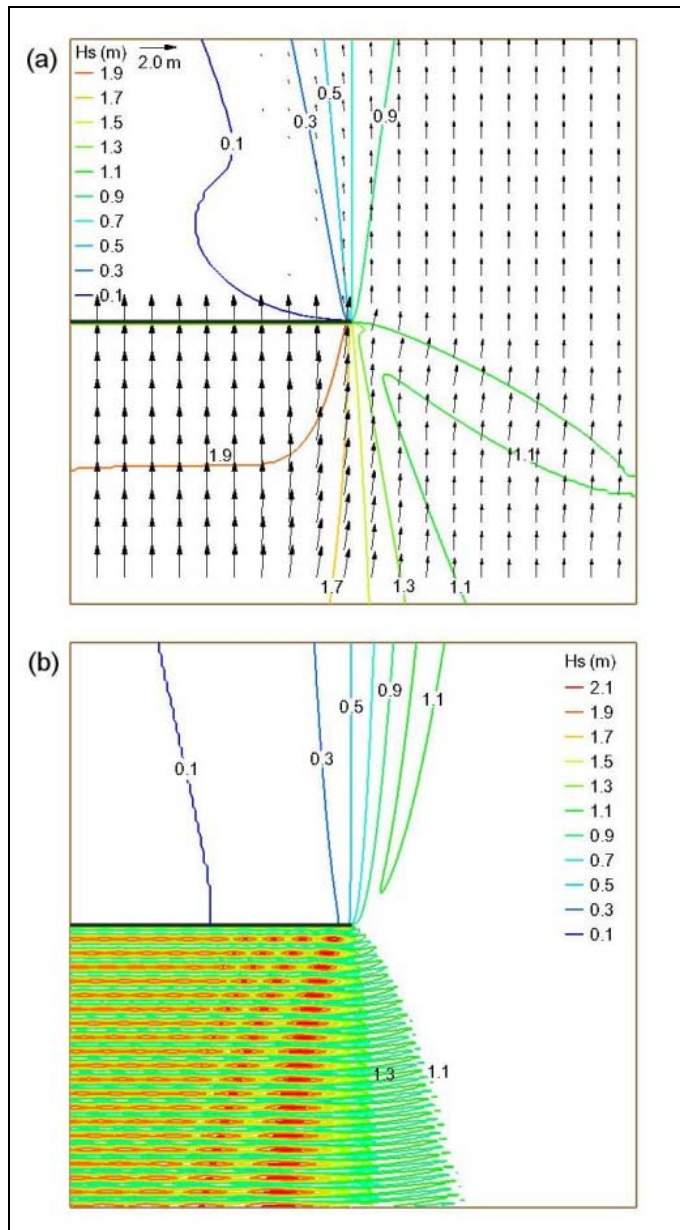


Fig. 1: (a) Calculated wave height (m) and approximate wave direction, and (b) analytical solution of wave height distribution for incident waves of 1 m, 8 sec, and 90-deg approach angle normal to fully reflective semi-infinite breakwater.

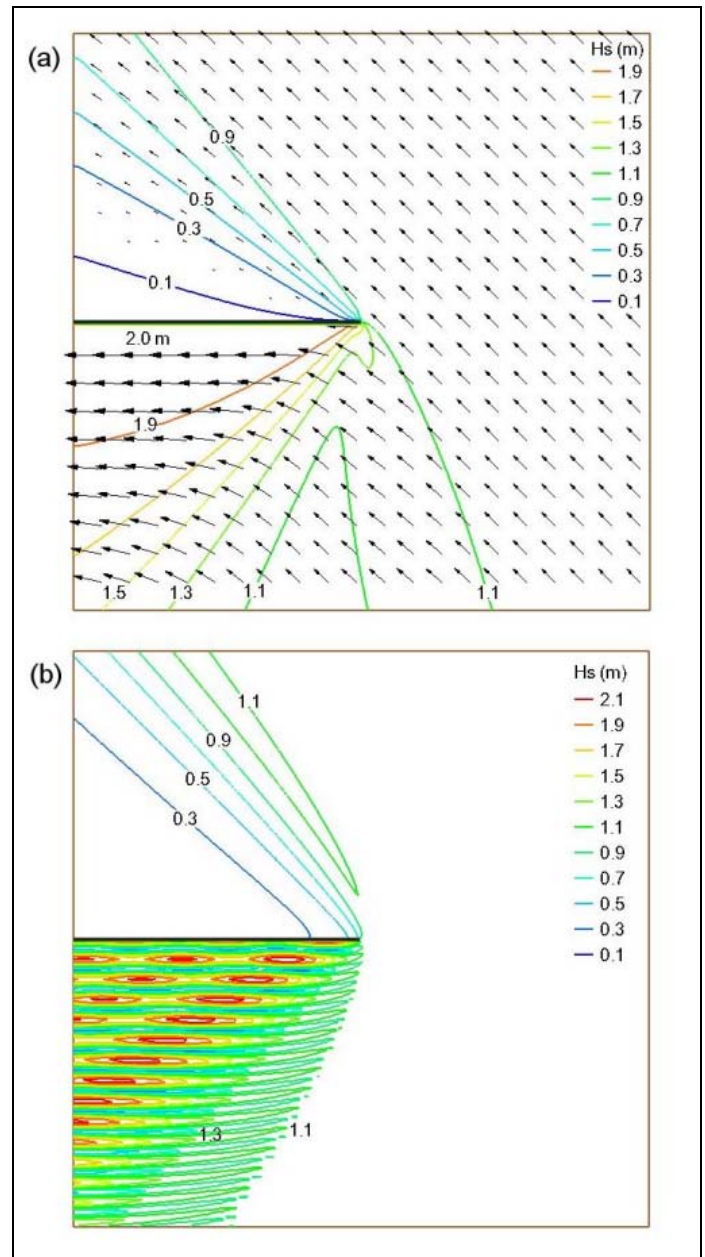


Fig. 2: (a) Calculated wave height (m) and approximate wave direction, and (b) analytical solution of wave height distribution for incident waves of 1 m, 8 sec, and 135-deg approach angle oblique to fully reflective semi-infinite breakwater.

The model results show both the diffracted and reflected energy levels in the lee and front of the breakwater similar to the analytical solution. The model cannot calculate the standing wave pattern caused by wave reflection as shown in the analytical solution.

### An Idealized Elliptic Shoal

Vincent and Briggs (1989) have conducted a physical model study for wave diffraction-refraction at a mound on a flat bottom. The mound has an elliptical perimeter of  $(x'/3.05)^2 + (y'/3.96)^2 = 1$  where  $x'$  and  $y'$  are local coordinates in m with the shoal center at  $x' = y' = 0$ . The water depth (m) over the shoal is given by

$$0.9144 - 0.6096 \sqrt{1.5625 - \left(\frac{x'}{3.05}\right)^2 - \left(\frac{y'}{3.96}\right)^2}$$

with the smallest depth equal to 0.1524 m at the center of shoal. The surrounding flat bottom has a constant depth of 0.4572 m.

The elliptical shoal experiment was conducted in a wave basin of 29-m long by 35-m wide. The long axis ( $y'$ -axis) of the mound is parallel to the wave generator approximately aligned with the global  $y$ -axis. The incident wave normal direction is parallel to the global  $x$  and local  $x'$  axis. The center of the shoal is located at  $x = 6.1$  m and  $y = 13.72$  m in the global coordinate system. Fig. 3 show the locations of elliptical shoal and nine transect lines for wave measurements.

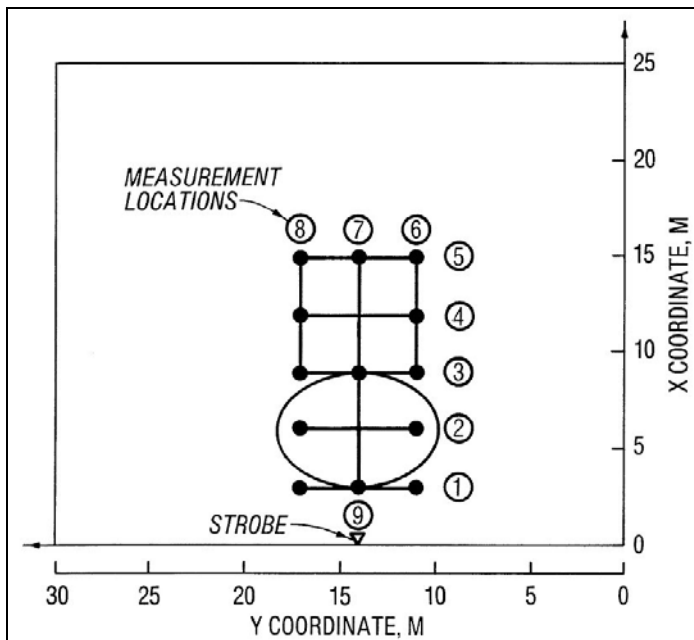


Fig. 3: Locations of elliptical shoal and measurement transects.

The elliptical shoal experiment consisted of 18 incident wave conditions to investigate different factors, including directional spreading, wave randomness, and wave breaking over the shoal. To demonstrate numerical modeling of combined diffraction-refraction, three incident wave conditions, named as B2, N2 and N4, for narrow frequency spectra were simulated. While B2 is associated with a symmetric and broad directional spreading, N2 and N4 are associated with a relatively narrow directional distribution. Table 1 presents the incident wave height  $H_s$ , spectral peak period  $T_p$ , spectral peak-enhancement factor  $\gamma$ , mean direction  $\theta_o$ , and directional spreading standard deviation  $\theta_s$  for B2, N2, and N4 (Vincent and Briggs, 1989).

Incident wave condition N4 is for non-breaking test with a wave height three times smaller than B2 and N2. The model simulations were performed at the laboratory scale. The model domain was a rectangular grid of  $25.1 \text{ m} \times 27.5 \text{ m}$  consisting of  $251 \times 275$  cells with cell size of  $0.1 \text{ m} \times 0.1 \text{ m}$ . The spectral wave transformation is computed on 27-frequency bins (0.6 to 0.99 Hz with 0.015-Hz increment) and 35-direction bins (covering a half-plane with 5-deg spacing). The simulations include cases with wave refraction only and with combined diffraction-refraction (use  $\epsilon = 0.0001$  for the diffraction calculation).

Table 1. Incident wave conditions B2, N2, and N4

Case ID	$H_s$ (m)	$T_p$ (sec)	$\gamma$	$\theta_o$ (deg)	$\theta_s$
B2	0.0775	1.3	20	0	30
N2	0.0775	1.3	20	0	10
N4	0.0254	1.3	20	0	10

Figs. 4 and 5 show calculated wave heights and directions with the outline of elliptical shoal and transect locations for B2 and N2, respectively. The model results show stronger wave energy focusing behind the shoal for a narrower frequency spectrum. Figs. 6 and 7 show calculated wave heights and data at Transects 3 and 4 for B2 and N2, respectively. Fig. 8 shows calculated wave height and data at Transect 4 for N4 (wave data for N4 available only at Transect 4).

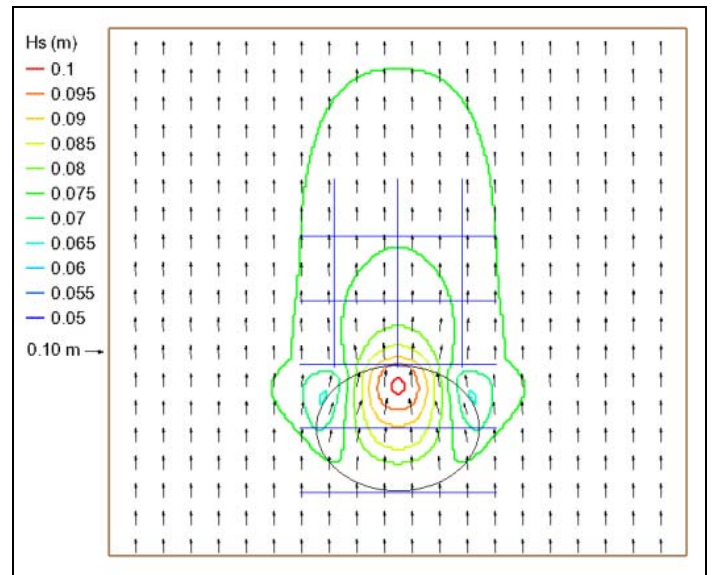


Fig. 4: Calculated wave height contours and vectors for for B2 with elliptical shoal outline (black) and transect lines (blue).

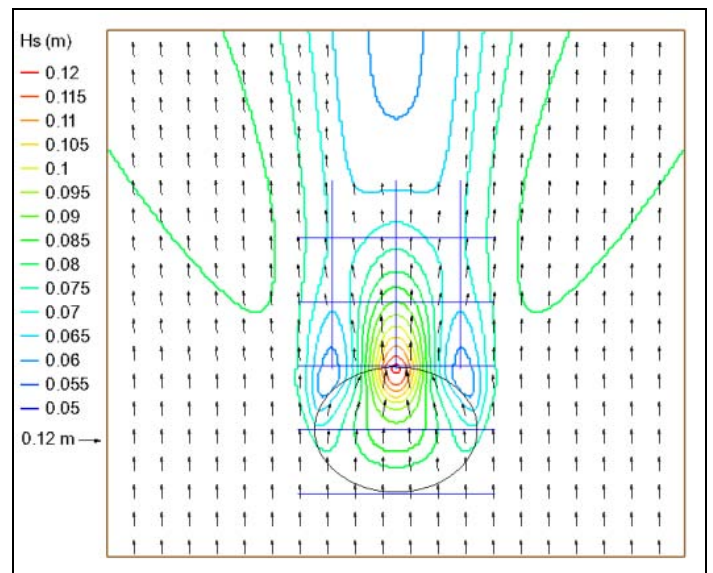


Fig. 5: Calculated wave height contours and vectors for N2 with elliptical shoal outline (black) and transect lines (blue).

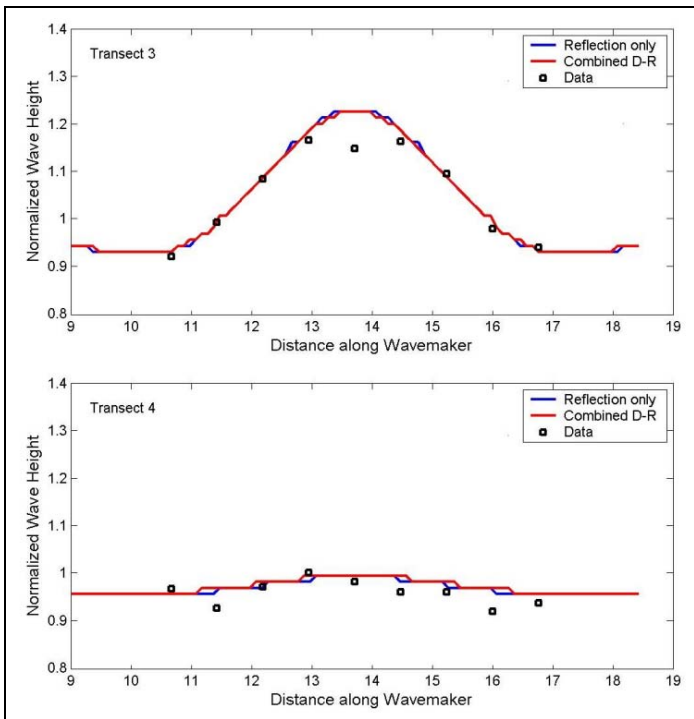


Fig. 6: Calculated wave heights and data at Transects 3 and 4 for B2 (D-R stands for diffraction-refraction).

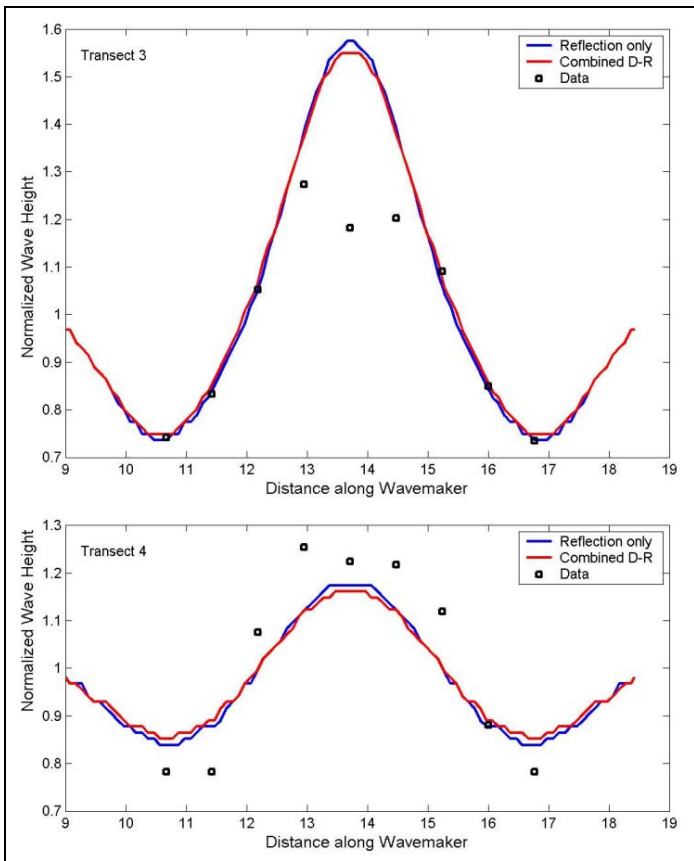


Fig. 7: Calculated wave heights and data at Transects 3 and 4 for N2 (D-R stands for diffraction-refraction).

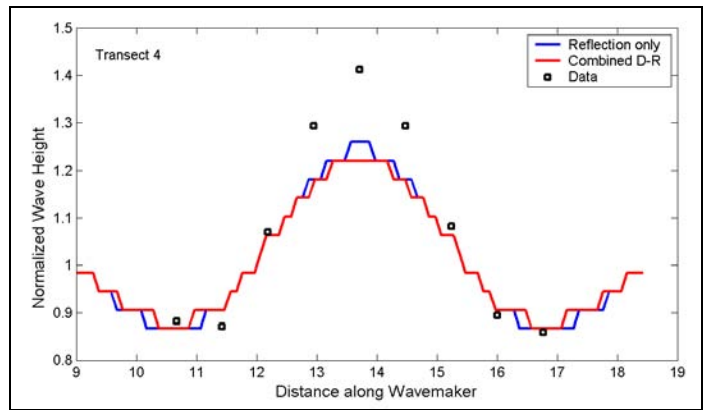


Fig. 8: Calculated wave heights and data at Transect 4 for N4 (D-R stands for diffraction-refraction).

The model results show small difference between runs with refraction only and with combined diffraction-refraction (D-R). This indicates that wave processes over the shoal is dominated mainly by refraction, and diffraction can be negligible. For B2, the model wave height agrees with data at Transects 3 and 4. For N2, the model calculated higher wave height at the middle of Transect 3 and lower wave height at the middle of Transect 4. For N4, of which the wave data is available only at Transect 4, the model also predicted lower wave height at the middle of Transect 4.

The difference between model calculated wave height and data behind the shoal may come from several reasons. First, the model wave height conversion from total local wave energy, i.e., Eq. 19, based on the linear wave theory may not be valid behind the shoal where wave activity is highly nonlinear. Second, wave data analyzed by conventional Fourier transform or zero-crossing wave height method may not be reliable for strong nonlinear waves behind the shoal. Third, the narrow directional spreading of spectral waves in N2 and N4 may not be accurately produced in the physical or numerical model. These factors cause the difference between model wave height and data.

### Cleveland Harbor, OH, Model

A 1:100-scale physical model experiment of Cleveland Harbor, Ohio, was conducted in 1980-1981 at the US Army Corps of Engineers Waterways Experiment Station to investigate waves, currents, water levels, and river flow on ship maneuverability (Bottin, 1983) in the harbor entrance and within the harbor complex. The harbor, located on the south shore of Lake Erie, is protected by two breakwaters with a combined length over 10 km (6 mile). The east breakwater consists of rubble mound stone and the west breakwater is mainly composed of concrete caisson. The Harbor has two entrances: the main entrance is located lakeward of the Cuyahoga River Mouth and the east entrance is at the eastern end of the east breakwater. Fig. 9 shows the harbor main entrance area.

The wave model grid was oriented East-West with the offshore boundary located approximately along the 16-m depth contour, and extended from the most westward to the furthest eastward ends of the Cleveland Harbor complex (Fig. 10). The wave model simulation was run in the prototype as the laboratory data were made available in the prototype scale. The model rectangular domain is 8.6 km  $\times$  20 km (172 square km), consisting of 860  $\times$  2000 cells with a uniform cell size of 10 m  $\times$  10 m.

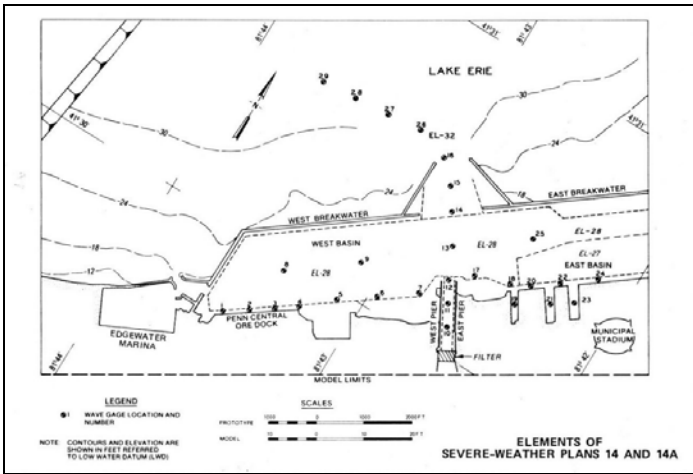


Fig. 9: Physical model of Cleveland Harbor main entrance and wave/current data collection locations.

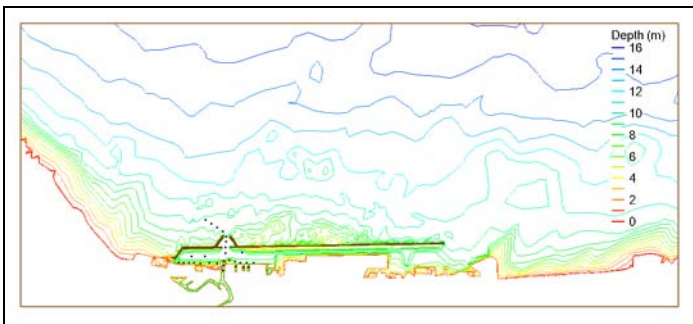


Fig. 10: Numerical wave model domain for Cleveland Harbor; black dot denotes wave/current gauge location.

The spectral wave transformation is computed with 30-frequency bins (0.04 to 0.33 Hz with 0.01-Hz increment) and 35-direction bins (covering a half-plane with 5-deg spacing). A constant Manning  $n = 0.025$  was used for bottom friction. The diffraction and reflection are calculated with  $\epsilon = 0.0001$  and a reflection coefficient = 0.5. Wave-current interaction feature, infra-gravity wave, wave transmission, and wave overtopping of breakwaters were triggered in the model (Lin et al. 2011a). The experiment tested 126 cases, consisting of 20 incident wave heights (monochromatic wave), 12 wave periods, 3 wave directions (unidirectional), 3 lake water levels, and two river discharges. For demonstration of modeling combined diffraction-refraction, a most probable incident wave condition of 3.14-m and 8-sec at the normal (mean) lake level with wave direction nearly perpendicular to long breakwaters and a strong river influx of 227- $m^3/sec$  (8,000-cfs) is simulated. The background steady-state current field is supplied by a CMS flow model (Lin et al. 2011b).

Figs. 11 and 12 show calculated wave fields in the harbor main entrance with and without the diffraction calculation, respectively. There are significant differences between model calculated wave height and spatial variation of wave fields with and without diffraction calculation in the main entrance channel. Fig. 13 compares the model calculated wave height with data for simulations with and without the diffraction calculation. A 45-deg line shown in the figure indicates a perfect match between calculated and measured wave heights. The model wave height calculated with combined diffraction-refraction agrees better with data than the calculation without the diffraction. This is especially true for large waves interacting with strong current from river influx in the main entrance channel.

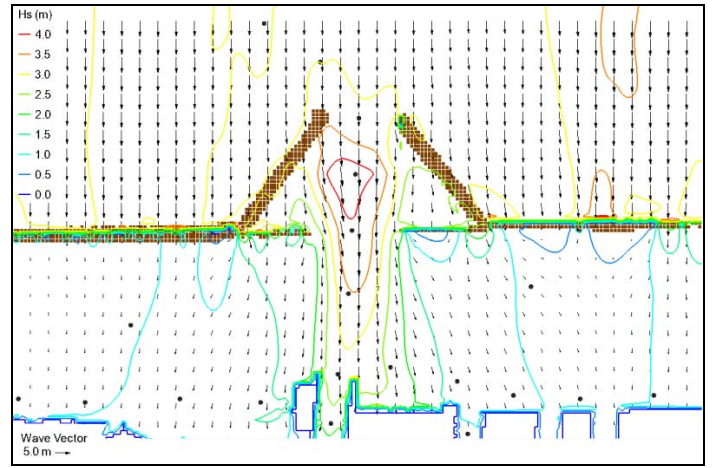


Fig. 11: Calculated wave heights and directions without diffraction calculation; black dot denotes wave/current gauge location.

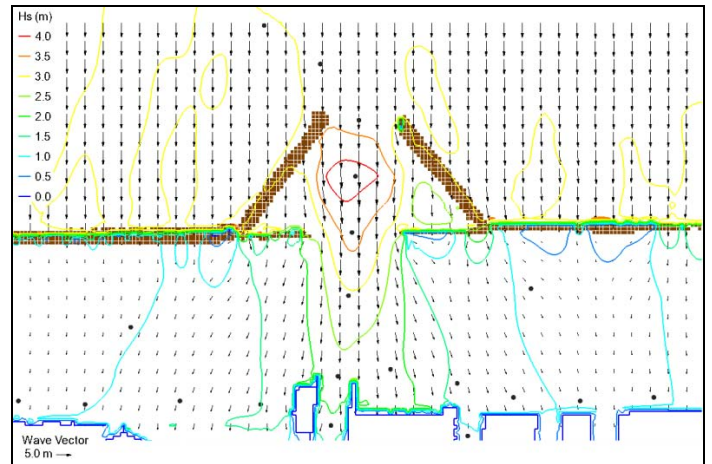


Fig. 12: Calculated wave field with combined diffraction-refraction calculation; black dot denotes wave/current gauge location.

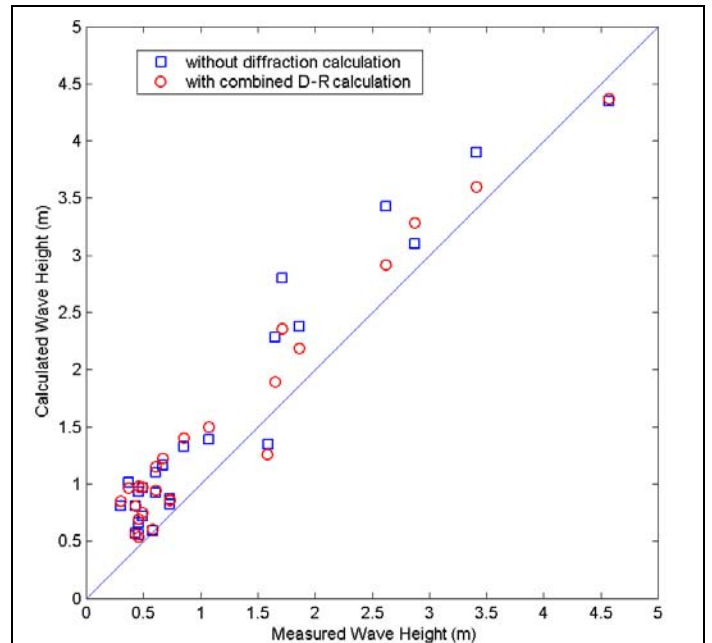


Fig. 13: Cleveland Harbor calculated wave height and data comparison.

## CONCLUSIONS

A theoretically-based wave diffraction formulation is provided in the wave-action balance equation for spectral wave modeling. The wave diffraction is combined with refraction and other coastal wave processes including reflection, wave-current interaction, and wave-structure interaction, etc. This spectral wave diffraction formulation is based on the classical Helmholtz equation that does not require additional mathematical approximations for surface wave interaction with structures. The combined diffraction-reflection calculation is demonstrated for an idealized long wedge, an elliptical shoal laboratory experiment, and a physical model of Cleveland Harbor, OH. The numerical simulations are performed using a 2D steady-state wave spectral transformation model for inlet applications in the Coastal Modeling System (CMS) of the US Army Engineer Research and Development Center. The numerical solution scheme for the model governing equation is computationally robust and stable. The case of idealized long wedge with the wedge angle of 0 represents a fully reflective semi-infinite breakwater. The analytical solution exists for the long vertical wedge that includes both wave diffraction and reflection. Two wave approach directions were simulated: perpendicular to the breakwater and 135-deg oblique incident direction. The model results show sufficient spectral wave diffraction and reflection in the lee and front of breakwater. The model wave height calculated from the total local wave energy is consistent with the analytical solution. Because spectral wave model does not calculate wave phase, it cannot capture full or partial standing wave patterns developed in the areas with reflected waves.

Model simulations for the elliptical shoal at the laboratory scale show that wave processes at the submerged shoal is mainly dominated by wave refraction, and diffraction can be negligible. Three incident wave conditions for narrow-band frequency spectra were simulated: one with a broad directional spreading, and the other two with same narrow directional distribution but different incident wave height. The model results for the broad directional spreading agree with data behind the shoal. In the case of incident waves with narrow directional spreading, the model tends to under-predict the wave height behind the shoal. This difference between model calculated wave height and data behind the shoal may come from the fact that the spectral wave model cannot accurately predict highly nonlinear and narrow directional spreading waves behind the shoal. The technical difficulty to generate accurately spectral waves with narrow directional spreading in the physical model may also be a contributor to the difference between model calculated wave height and data.

The physical model of Cleveland harbor, OH, is more for the real world condition with combined coastal wave processes including diffraction, refraction, reflection, bottom friction, wave overtopping rubble-mound and vertical-wall breakwaters, and wave-current interaction at various wave levels. The model simulation includes a storm wave condition at the mean water level with a strong river influx in the back side of the harbor. The model results were compared with and without diffraction calculation. The model wave heights calculated with combined diffraction-refraction agree better with data than without the diffraction, especially for large waves interacting with strong current in the main entrance channel.

The examples of model simulations given in the present paper are intended for the demonstration purpose because the spectral wave models can only calculate the change and transformation of the local wave energy but not the wave phase information. Therefore, the model calculated wave height is only meaningful to show the local wave energy level and by no means to represent the actual wave height

observed in the physical model or measured in the field. The difference between model calculated wave height and data is evident behind a shoal or in front of a reflective wall that full or partial standing waves occur with crossing waves from different directions.

## ACKNOWLEDGEMENTS

The authors are grateful to Drs. Julie D. Rosati and Nicholas C. Kraus for their continual encouragement and support towards development and improvement of the spectral wave transformation capabilities to increase the reliability of wave modeling for coastal inlets and navigation applications. Permission was granted by the Chief, U. S. Army Corps of Engineers to publish this information.

## REFERENCES

- Berkhoff, JCW (1972). "Computation of combined refraction-diffraction," *Proc 13th Conf. Coastal Eng., ASCE*, Vancouver.
- Berkhoff, JCW, Booij, N, and Radder, AC (1982). "Verification of numerical wave propagation models for simple harmonic linear water waves," *Coastal Eng.*, 6, pp 255-279.
- Bottin, Jr. RR (1983). Cleveland Harbor, Ohio, design for the safe and efficient passage of 1000-ft-long vessels at the west (main) entrance. Technical Report HL-83-6, Vicksburg, MS: U.S. Army Engineer Waterways Experiment Station, 346 pp.
- Cartwright, DE, and Longuet-Higgins, MS (1956). "The statistical distribution of the maxima of random function," *Proc. Roy.Soc. London, Ser. A.*, Vol. 237, pp 212-232.
- Chawla, A, Ozkan-Haller, HT, and Kirby, JT (1988). "Spectral model for wave transformation and breaking over irregular bathymetry," *J. Waterway, Port, Coastal, Ocean Eng.*, 124:4, pp 189-198.
- Chen, HS (1987). Combined reflection and diffraction by a vertical wedge. Technical Report CERC-87-16, Vicksburg, MS: US Army Engineer Waterways Experiment Station, 75 pp.
- Donelan, MA, Hamilton, J, and Hui, WH (1985). "Directional spectra of wind-generated waves," *Phil. Trans. Math. Comp.*, 19, pp 297-301.
- Lin, L, Demirebilek, Z, Mase, H, Zheng, J, and Yamada, F (2008). CMS-Wave: A nearshore spectral wave processes model for coastal inlets and navigation projects. ERDC/CHL TR-08-13, Vicksburg, MS: U.S. Army Engineer Research and Development Center, 131 pp.
- Lin, L, Demirebilek, Z, and Mase, H (2011a). "Recent capabilities of CMS-Wave: A coastal wave model for inlets and navigation projects," Symposium to honor Dr. Nicholas Kraus. *Proc. Journal of Coastal Research*, Special Issue 59, pp 7-14.
- Lin, L, Demirebilek, Z, Thomas, R, and Rosati III, J (2011b). Verification and validation of the Coastal Modeling System, Report 2: CMS-Wave. ERDC/CHL TR-11-10, Vicksburg, MS: U.S. Army Engineer Research and Development Center, 111 pp.
- Mase, H (2001). "Multidirectional random wave transformation model based on energy balance equation," *Coastal Eng.*, JSCE. 43(4) pp 317-337.
- Nwogu, O, and Demirebilek, Z (2001). BOUSS-2D: A Boussinesq wave model for coastal regions and harbors. ERDC/CHL TR-01-25, Vicksburg, MS: US Army Engineer Research and Development Center, 92 pp.
- Penny, WG, and Price, AT (1944). Diffraction of water waves by breakwaters. Misc. Weapons Development Technical History 26, Artificial Harbors, Sec. 3D.
- Sommerfeld, A (1896). "Mathematische theorie der diffraction," *Math. Ann.*, Vol. 47, pp 317-374.
- Vincent, CL, and Briggs, MJ (1989). "Refraction-diffraction of irregular waves over a mound," *Journal of Waterway, Port, Coastal and Ocean Eng.*, Vol. 115, pp 269-284.